ChemComm

COMMUNICATION

View Article Online
View Journal | View Issue

Cite this: *Chem. Commun.*, 2025, **61**, 3844

Received 3rd January 2025,
Accepted 4th February 2025

DOI: 10.1039/d4cc06797e

rsc.li/chemcomm

Highly conductive and homogeneous NiO_x nanoparticles for stable and efficient flexible perovskite solar cells†

Junjun Jin,‡[a] Jitao Shang,‡[a] Zhenkun Zhu,[a] Tonghui Guo,[a] Yanghou Wang,[b] Lijun Chen,[b] Yidong Ming,[c] Jinhua Li,[c] Guanqi Tang*[b] and Qidong Tai*[a]

We present a facile strategy to improve the conductivity and homogeneousness of nickel oxide nanoparticles (NiO_x NPs). The inverted flexible perovskite solar cells (F-PSCs) prepared with NiO_x achieved impressive efficiencies of 22.68% under AM 1.5G and 35.59% under 1000 lux, respectively.

With advancements in electronic technology, the growing demand for unmanned systems, building-integrated photovoltaics, portable electronics, smart textiles, and the Internet of Things (IoT) highlights the significant potential of F-PSCs as efficient power sources.[1–4] F-PSCs are especially suitable for such applications due to their high power conversion efficiency (PCE), cost-effective manufacturing, light-weight structure, and exceptional flexibility.[5–7]

NiO_x has been considered as a promising HTL in F-PSCs due to its excellent optical transparency, chemical stability, and suitable work function with perovskites.[8,9] F-PSCs with p–i–n device structure, utilizing NiO_x as the HTL, exhibit minimal hysteresis and long-term stability. Currently, NiO_x HTLs can be fabricated using methods such as atomic layer deposition (ALD), pulsed laser deposition (PLD), sputtering, and sol–gel coating.[10] Nonetheless, the stringent preparation conditions (high-temperature annealing and/or high vacuum) hinder their large-scale application and make them unsuitable for flexible substrates. NiO_x HTLs can be processed using synthetic NiO_x NPs, which are obtained by synthesizing $Ni(OH)_2$ through the chemical precipitation of nickel nitrate ($Ni(NO_3)_2$) and alkali, followed by calcination.[11] NiO_x NPs can be easily used to prepare HTLs for F-PSCs by solution processing. However, NiO_x NPs synthesized by this method usually exhibit low intrinsic conductivity.[12,13] Additionally, the $Ni(OH)_2$ formed through reaction precipitation exhibits an uneven crystal grain size distribution due to the inconsistent rate of reaction precipitation (first fast and then slow), which further results in varying crystal grain sizes of the NiO_x NPs.[14] During the dispersion process, smaller particles tend to adsorb onto the surface of larger particles, leading to agglomeration and resulting in a rough NiO_x film.[15] This poor surface morphology causes inadequate interfacial contact with the perovskite film, ultimately limiting the efficiency and stability of the prepared F-PSCs.[16,17] However, current research on NiO_x NPs primarily focuses on enhancing conductivity through doping, with limited attention to the uniformity of NiO_x NPs.[9,10]

In this work, we introduce a new method for obtaining highly conductive and homogeneous NiO_x NPs *via* an oxidant-assisted method using ammonium persulfate (APS). Specifically, APS is added to the $Ni(NO_3)_2$ precursor solution, where it oxidizes Ni^{2+} into nickel oxide hydroxide (NiOOH), as shown in Fig. 1. This process slows the initial reaction rate for forming nickel hydroxide ($Ni(OH)_2$) NPs, promotes the formation of smaller and more uniform $Ni(OH)_2$ NPs, and facilitates the synthesis of well-dispersed NiO_x NPs with smaller and more uniform crystal grain sizes. Additionally, NiOOH increases the Ni^{3+} content in the prepared NiO_x NPs, which helps improve their intrinsic conductivity. Adjusting the Ni^{3+} content can also optimize the energy levels of NiO_x NPs, minimizing energy loss at the NiO_x/perovskite interface. Ultimately, the PCE of inverted F-PSCs prepared with the optimized NiO_x HTL reaches 22.68%

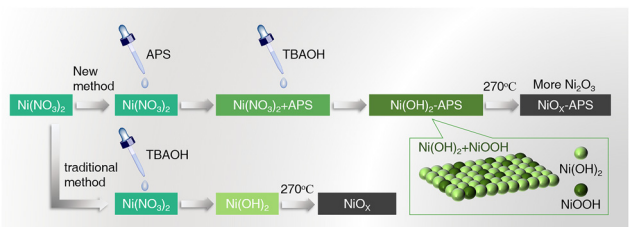

Fig. 1 Synthesis illustration of NiO_x and NiO_x–APS nanoparticles.

[a] *The Institute of Technological Sciences, Wuhan University, Wuhan 430072, P. R. China. E-mail: qdtai@whu.edu.cn*
[b] *Research Institute of Frontier Science, Southwest Jiaotong University, Chengdu 610500, P. R. China. E-mail: guanqitang13@swjtu.edu.cn*
[c] *School of Materials Science and Engineering, Hubei University, Wuhan 430062, P. R. China*

† Electronic supplementary information (ESI) available. See DOI: https://doi.org/10.1039/d4cc06797e

‡ These authors contributed equally to this work.

under AM 1.5G and 35.59% under 1000 lux. Furthermore, the optimized device retains 92% of its efficiency after 1000 bending cycles and 91% of its initial efficiency after 1000 hours of unpackaged storage.

As illustrated in Fig. 1, the $Ni(OH)_2$ and NiO_x NPs prepared using the new method are denoted as $Ni(OH)_2$–APS and NiO_x–APS, respectively (0.3 mol% APS was added to the $Ni(NO_3)_2$ precursor solution, with the dosage preliminarily optimized, as detailed in Fig. S1 and Table S1 (ESI†)). As presented in transmission electron microscopy (TEM) images (Fig. 2a–d), the control $Ni(OH)_2$ exhibits large crystal sizes, broad size distribution, and significant aggregation. In contrast, the APS-assisted synthesis of $Ni(OH)_2$–APS results in smaller crystal size, narrower size distribution, and the absence of aggregation. Similarly, the NiO_x and NiO_x–APS, derived from $Ni(OH)_2$ and $Ni(OH)_2$–APS, respectively, display similar improvements. As shown in Fig. 2e–h, NiO_x–APS demonstrates more uniform and smaller crystal size compared to control NiO_x, with the average crystal sizes of 6.42 nm and 9.85 nm, respectively (see the statistical size distribution in Fig. S2, ESI†). This improvement is attributed to the addition of APS into the $Ni(NO_3)_2$ precursor solution, which triggers a new chemical reaction:

$$2Ni(NO_3)_2 + (NH_4)_2S_2O_8 + 2TBAOH \rightarrow 2NiOOH + 2NH_4NO_3 + (TBA)_2SO_4.$$

The reaction reduced the initial rate of the original chemical reaction ($Ni(NO_3)_2$ + 2TBAOH → $Ni(OH)_2$ + 2$TBANO_3$), leading to a more uniform precipitation rate for $Ni(OH)_2$ formation. Furthermore, the NiOOH generated in the new reaction effectively prevented the accumulation of $Ni(OH)_2$ NPs caused by uneven crystal grain sizes, thereby facilitating the formation of $Ni(OH)_2$–APS NPs with smaller and more homogeneous crystal grain sizes. This further determines the morphology of NiO_x NPs after the sintering of $Ni(OH)_2$ NPs. Further X-ray diffraction (XRD) and Raman characterization revealed that the prepared NiO_x and NiO_x–APS NPs exhibit similar diffraction peaks, confirming their identical composition and structure (Fig. S3, ESI†).

The control $Ni(OH)_2$ and $Ni(OH)_2$–APS were further investigated by X-ray photoelectron spectroscopy (XPS). In the oxygen 1s spectrum (Fig. 2i and j), the two peaks at 532.2 eV and 530.8 eV correspond to NiOOH and $Ni(OH)_2$, respectively.[12,18] The NiOOH content in $Ni(OH)_2$–APS reaches 28.5%, significantly higher than the 14.8% observed in the control $Ni(OH)_2$. The NiOOH in the control $Ni(OH)_2$ NPs formed due to exposure to air during the reaction process, with a small amount of oxygen participating in the reaction. This confirms that APS promotes the formation of NiOOH from $Ni(NO_3)_2$.[10,19] Additionally, the dark green color of $Ni(OH)_2$–APS (Fig. S4, ESI†) also further supports this observation, as the control $Ni(OH)_2$ appears apple green, while NiOOH is black.[10] Notably, the characteristic peak of S 2p is absent in the $Ni(OH)_2$–APS XPS spectrum (Fig. S5, ESI†), indicating that APS is completely removed during the cleaning steps and does not affect the subsequent NiO_x preparation process. The new synthesis method primarily optimizes $Ni(OH)_2$, leading to small grain sizes and uniform NiO_x NPs.

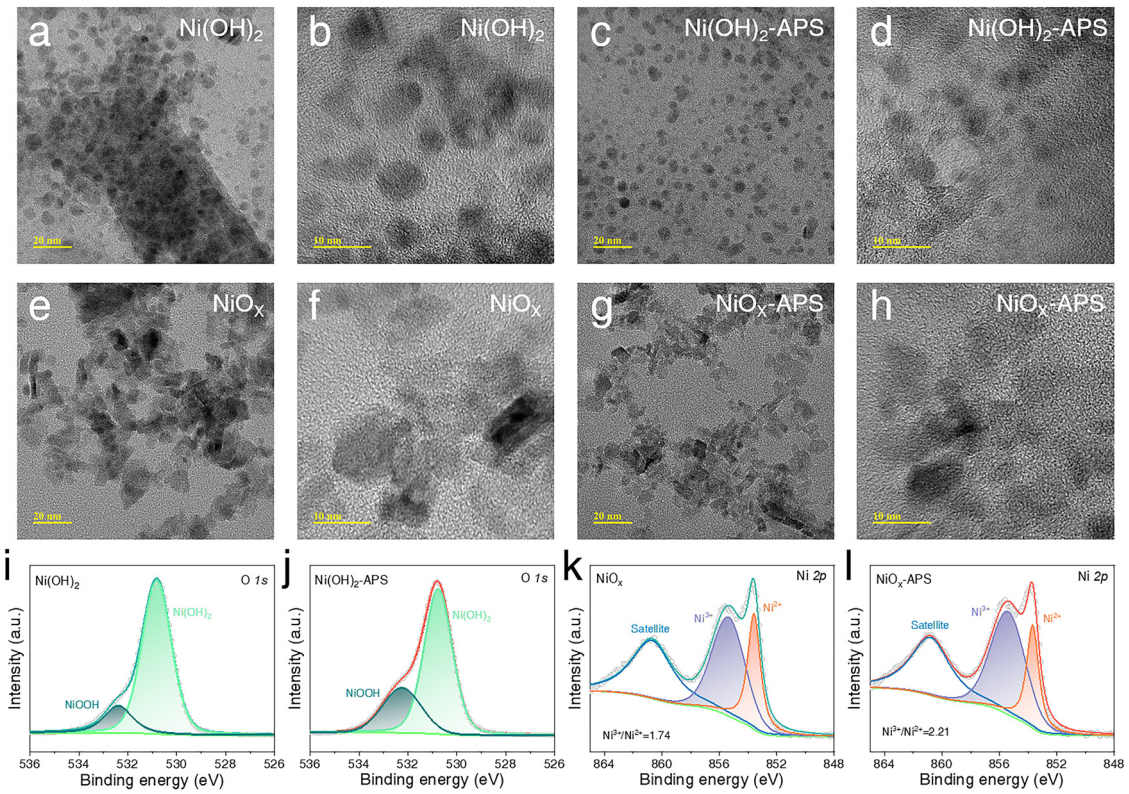

Fig. 2 (a)–(h) The TEM micrographs and magnified TEM micrographs of the as-prepared $Ni(OH)_2$, $Ni(OH)_2$–APS, NiO_x and NiO_x–APS NPs, respectively. (i) and (j) XPS O 1s spectra of $Ni(OH)_2$ and $Ni(OH)_2$–APS NPs. (k) and (l) XPS Ni 2P spectra of NiO_x and NiO_x–APS films.

The NiO_x and NiO_x–APS films were prepared by spin-coating onto flexible indium tin oxide (ITO)/polyethylene glycol terephthalate (PET) substrates using inks prepared from NiO_x NPs and NiO_x–APS NPs, respectively. As shown in the scanning electron microscopy (SEM) images (Fig. S6, ESI†), the NiO_x–APS film exhibits a flatter and smoother surface compared to the control NiO_x film, likely due to the smaller size and uniformity of the NiO_x–APS NPs. The chemical state of NiO_x–APS films was analyzed using XPS, and the results were compared to those of the NiO_x films (Fig. 2k and l). The NiO_x and NiO_x–APS films show the same characteristic peaks in the Ni 2p spectrum, with peaks at 855.5 and 853.6 eV corresponding to Ni^{3+} and Ni^{2+}, respectively.[14,20] Ni^{3+} is typically derived from Ni^{2+} vacancies at the grain boundaries of the oxygen-enriched NiO_x lattice, which enhances conductivity and facilitates hole transport.[18] The Ni 2p spectrum reveals that the Ni^{3+}/Ni^{2+} ratio in the NiO_x–APS film (2.21) is higher than that in the control NiO_x film (1.74), indicating enhanced hole transport and conductivity in the NiO_x–APS film. The O 1s spectrum (Fig. S7, ESI†) indicates that the increase in Ni^{3+} in NiO_x–APS films is attributed to the higher proportion of NiOOH.[20] Additionally, the smaller crystal grain sizes of $Ni(OH)_2$–APS NPs may contribute to the increase in Ni^{3+} by facilitating complete annealing in an oxygen-rich environment.[11]

The conductivity of NiO_x and NiO_x–APS films was calculated by measuring the current density–voltage (*J–V*) curves of devices with the structure of ITO/NiO_x or NiO_x–APS/Au (Fig. 3a). The calculated conductivity values of NiO_x and NiO_x–APS films are 1.19×10^{-2} mS cm^{-1} and 1.82×10^{-2} mS cm^{-1}, respectively.[21,22] Additionally, the conductive atomic force microscopy (c-AFM) images in Fig. 3b and c also indicated that NiO_x–APS film exhibits better conductivity and a more uniform current distribution compared to the control NiO_x film. To determine the hole mobility of NiO_x and NiO_x–APS films, we measured the space-charge-limited current of the devices with the structure of ITO/NiO_x or NiO_x–APS/spiro-OMeTAD/Au (Fig. 3d). The hole mobility increased from 9.2×10^{-4} cm^2 V^{-1} s^{-1} (NiO_x) to 2.6×10^{-3} cm^2 V^{-1} s^{-1} (NiO_x–APS), indicating improved charge transport in the NiO_x–APS films.[23]

The surface potential distribution of the NiO_x and NiO_x–APS films was studied *via* the Kelvin probe force microscope (KPFM). As shown in Fig. 3e and f, the contact potential difference (CPD) of NiO_x–APS films is lower than that of control NiO_x films, indicating a higher work function (W_F) for the NiO_x–APS films.[24,25] Furthermore, the energy levels of NiO_x and NiO_x–APS films were calculated using ultraviolet photoelectron spectroscopy (UPS) and ultraviolet-visible absorption spectra (UV-vis) (Fig. 3g, h and Fig. S8, ESI†). The resulting energy level diagram is shown in Fig. 3i. Compared to the control NiO_x film, the valence band (VB) of the NiO_x–APS film decreased from −5.29 eV to −5.45 eV, and the Fermi level (E_F) shifted from −4.54 eV to −4.76 eV, which was consistent with the KPFM results. Additionally, the VB of the NiO_x–APS film is closer to that of the perovskite film, facilitating hole transport and reducing energy loss.

The photovoltaic performance of devices with NiO_x and NiO_x–APS HTLs was evaluated in F-PSCs with an inverted structure of ITO/NiO_x or NiO_x–APS/PTAA/perovskite/PCBM/BCP/Ag, as illustrated in Fig. 4a. The PTAA is primarily aimed at passivating the NiO_x/perovskite interface. Fig. 4b shows the *J–V* curves of the optimized F-PSCs measured under AM 1.5G illumination, with detailed photovoltaic parameters listed in Table S2 (ESI†). The PCE of the device with NiO_x–APS HTL reached 22.68%, higher than the 19.63% for the device with the control NiO_x HTL. This efficiency is relatively higher compared to other f-PSC studies using NiO_x as the hole transport material (Table S3, ESI†). Moreover, the NiO_x–APS based devices exhibited negligible hysteresis. Fig. S9 (ESI†) shows the statistical photovoltaic performance of different devices (20 devices), with the distribution trends matching the changes observed in the optimal photovoltaic parameters. The PCE enhancement of the NiO_x–APS based devices is primarily attributed to improvements in open-circuit voltage (V_{OC}), short-circuit current density (J_{SC}), and fill factor (FF). The increase in J_{SC} of NiO_x–APS based devices is attributed to

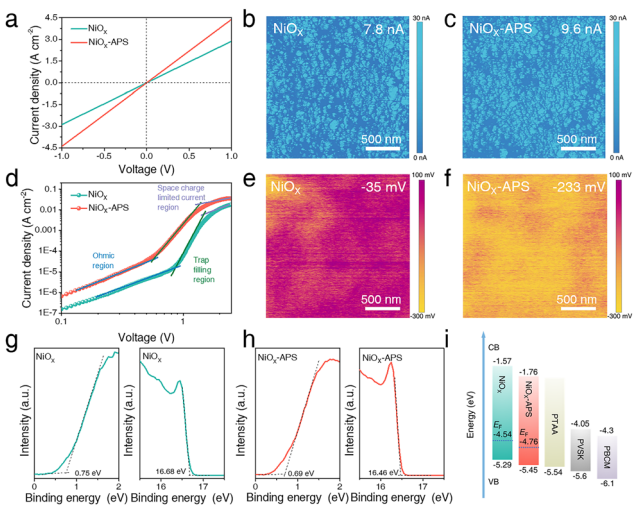

Fig. 3 (a) The *J–V* of the devices with the structure of ITO/NiO_x or NiO_x–APS/Au. (b) and (c) c-AFM images of NiO_x and NiO_x–APS film-coated ITO/PET. (d) The space-charge-limited current of hole-only devices with the structure of ITO/NiO_x or NiO_x–APS/spiro-OMeTAD/Au. (e) and (f) KPFM images of NiO_x and NiO_x–APS film-coated ITO/PET. (g) and (h) The UPS spectra of NiO_x and NiO_x–APS films. (i) Energy-level diagram of the PSCs.

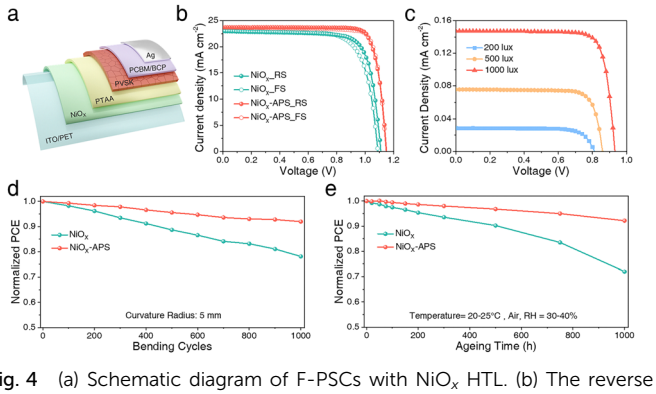

Fig. 4 (a) Schematic diagram of F-PSCs with NiO_x HTL. (b) The reverse and forward scanned *J–V* curves of the best-performed F-PSCs based on NiO_x and NiO_x–APS HTL. (c) The *J–V* curves of the best-performed F-PSCs based on NiO_x–APS HTL measured under different indoor light illumination. (d) Bending stability of F-PSCs with convex bending cycles at a curvature radius of 5 mm. (e) Long-term storage stability of the unencapsulated F-PSCs under air environments with RH of 30–40%.

the flatter and smoother surface of the NiO_x–APS films and the smaller contact angle (27°) of the perovskite precursor solution on the NiO_x–APS/PTAA film compared to the control NiO_x/PTAA film (32°), which promotes the formation of high-quality perovskite films (Fig. S10 and S11, ESI†). The improvements in V_{OC} and FF of NiO_x–APS based F-PSCs are due to the excellent conductivity of NiO_x–APS films and matched energy level, which helps reduce the series resistance (R_s) and increase the recombination resistance (R_{rec}) of the devices (Fig. S12, ESI†).[26,27] Furthermore, considering the suitability of F-PSCs for Internet of Things (IoT) applications,[28,29] we investigated the photovoltaic performance of NiO_x–APS-based F-PSCs under different indoor light intensities (Fig. S13, ESI†). Fig. 4c shows the *J*–*V* curves of the champion F-PSC, with high PCEs of 35.59%, 32.92%, and 28.28% under 1000 lux, 500 lux, and 200 lux, respectively (Table S4, ESI†).

Finally, to assess mechanical durability, F-PSCs with NiO_x and NiO_x–APS HTLs were subjected to repeated bending cycles with a 5 mm radius. Fig. 4d shows the PCE changes during the repeated F-PSC bending cycles. As the number of cycles increased, device performance gradually decreased. After 1000 bending cycles, the NiO_x–APS based F-PSCs retained 92% of their initial PCE, while the control NiO_x based F-PSCs retained only 78% of their PCE. This is attributed to the superior NiO_x/perovskite interfaces in NiO_x–APS based F-PSCs, compared to the significant gaps observed at the NiO_x/perovskite interfaces of control NiO_x-based F-PSCs, as shown in Fig. S10 (ESI†). During bending, these gaps in the control NiO_x-based F-PSCs are prone to cracking and slippage, compromising their bending stability. Additionally, NiO_x–APS based F-PSCs demonstrated excellent long-term stability (Fig. 4e), retaining 91% of their initial PCE after 1000 hours of storage for unpackaged devices in an environment with 30–40% relative humidity at room temperature. In contrast, the control NiO_x based F-PSCs retained only 72% of their PCE.

In summary, we have innovatively synthesized NiO_x–APS NPs to achieve high conductivity and a uniformly flat HTL in F-PSCs. Compared to reference devices, inverted F-PSCs based on the NiO_x–APS HTL exhibit superior photovoltaic performance, with a PCE of 22.68% under AM 1.5G and 35.59% under 1000 lux illumination. Furthermore, NiO_x–APS based F-PSCs demonstrate remarkable operational and mechanical stability. This study offers a pathway to advancing high-performance F-PSCs and provides a new approach to enhancing HTL performance.

This work was financially supported by the National Natural Science Foundation of China (No. 61974106, 62304185). The authors thank Dr Xiaodong Zhou from the Core Facility of Wuhan University for their assistance with c-AFM, KPFM measurements and data analysis.

Data availability

The authors confirm that data supporting the findings of this study are available in the article and ESI.†

Conflicts of interest

There are no conflicts to declare.

Notes and references

1 M. Z. Qamar, Z. Khalid, R. Shahid, W. C. Tsoi, Y. K. Mishra, A. K. K. Kyaw and M. A. Saeed, *Nano Energy*, 2024, **129**, 109994.
2 Q. Zhou, X. Liu, Z. Liu, Y. Zhu, J. Lu, Z. Chen, C. Li, J. Wang, Q. Xue, F. He, J. Liang, H. Li, S. Wang, Q. Tai, Y. Zhang, J. Liu, C. Zuo, L. Ding, Z. Xiong, R. Zheng, H. Zhang, P. Zhao, X. Jin, P. Wu, F. Zhang, Y. Jiang, H. Zhou, J. Hu, Y. Wang, Y. Song, Y. Mai, B. Xu, S. Liu, L. Han and W. Chen, *Mater. Futures*, 2024, **3**, 022102.
3 B. Xia, J. Jin, N. Wang and Q. Tai, *Adv. Funct. Mater.*, 2024, **34**, 2308581.
4 Z. Sun, Y. Huang, J. Kong, J. Tang and Z. Du, *Chem. Commun.*, 2025, **61**, 1243–1261.
5 G. Tang and F. Yan, *Nano Today*, 2021, **39**, 101155.
6 F. Song, D. Zheng, J. Feng, J. Liu, T. Ye, Z. Li, K. Wang, S. Liu and D. Yang, *Adv. Mater.*, 2024, **36**, 2312041.
7 J. Jin, J. Li, Q. Tai, Y. Chen, D. D. Mishra, W. Deng, J. Xin, S. Guo, B. Xiao and X. Wang, *J. Power Sources*, 2021, **482**, 228953.
8 Y. Li, H. Wu, W. Qi, X. Zhou, J. Li, J. Cheng, Y. Zhao, Y. Li and X. Zhang, *Nano Energy*, 2020, **77**, 105237.
9 F. Ma, Y. Zhao, J. Li, X. Zhang, H. Gu and J. You, *J. Energy Chem.*, 2021, **52**, 393–411.
10 H. Zhang, C. Zhao, J. Yao and W. C. H. Choy, *Angew. Chem., Int. Ed.*, 2023, **62**, 202219307.
11 X. Cui, J. Jin, J. Zou, Q. Tang, Y. Ai, X. Zhang, Z. Wang, Y. Zhou, Z. Zhu, G. Tang, Q. Cao, S. Liu, X. Liu and Q. Tai, *Adv. Funct. Mater.*, 2022, **32**, 2203049.
12 Y. Liu, B. Ding, G. Zhang, X. Ma, Y. Wang, X. Zhang, L. Zeng, M. K. Nazeeruddin, G. Yang and B. Chen, *Adv. Sci.*, 2024, **11**, 2309111.
13 L. Tian, R. Tyburski, C. Wen, R. Sun, M. Abdellah, J. Huang, L. D'Amario, G. Boschloo, L. Hammarström and H. Tian, *J. Am. Chem. Soc.*, 2020, **142**, 18668–18678.
14 X. Tong, F. Li, J. Jin, X. Guo, J. Li, F. Yan, X.-Z. Zhao and Q. Tai, *J. Phys. D: Appl. Phys.*, 2021, **54**, 144002.
15 S. Zhang, H. Wang, X. Duan, L. Rao, C. Gong, B. Fan, Z. Xing, X. Meng, B. Xie and X. Hu, *Adv. Funct. Mater.*, 2021, **31**, 2106495.
16 X. Duan, Z. Huang, C. Liu, J. Yang, L. Tan and Y. Chen, *Chem. Commun.*, 2019, **55**, 3666–3669.
17 Y. Zhou, T. Guo, J. Jin, Z. Zhu, Y. Li, S. Wang, S. Zhou, Q. Lin, J. Li, W. Ke, G. Fang, X. Zhang and Q. Tai, *Energy Environ. Sci.*, 2024, **17**, 2845–2855.
18 S. Yu, Z. Xiong, H. Zhou, Q. Zhang, Z. Wang, F. Ma, Z. Qu, Y. Zhao, X. Chu, X. Zhang and J. You, *Science*, 2023, **382**, 1399–1404.
19 N. Tiwari, H. Arianita Dewi, E. Erdenebileg, R. Narayan Chauhan, N. Mathews, S. Mhaisalkar and A. Bruno, *Sol. RRL*, 2021, **36**, 2100700.
20 J. Zhang, J. Yang, R. Dai, W. Sheng, Y. Su, Y. Zhong, X. Li, L. Tan and Y. Chen, *Adv. Energy Mater.*, 2022, **12**, 2103674.
21 S. Wang, Y. Li, J. Yang, T. Wang, B. Yang, Q. Cao, X. Pu, L. Etgar, J. Han, J. Zhao and X. Li, *Angew. Chem., Int. Ed.*, 2022, **61**, 202116534.
22 W. Feng, X. Liu, G. Liu, G. Yang, Y. Fang, J. Shen, B. Jin, X. Chen, Y. H. Huang, X. D. Wang, C. Wu, S. Yang and W. Q. Wu, *Angew. Chem., Int. Ed.*, 2024, **63**, e202403196.
23 J. Yang, T. Wang, Y. Li, X. Pu, H. Chen, Y. Li, B. Yang, Y. Zhang, J. Zhao, Q. Cao, X. Chen, S. Ghasemi, A. Hagfeldt and X. Li, *Sol. RRL*, 2022, **6**, 2200422.
24 C. Li, Y. Zhang, X. Zhang, P. Zhang, X. Yang and H. Chen, *Adv. Funct. Mater.*, 2023, **33**, 2214774.
25 G. Liu, G. Yang, W. Feng, H. Li, M. Yang, Y. Zhong, X. Jiang and W. Q. Wu, *Adv. Mater.*, 2024, **36**, 2405860.
26 L. Lin, J. T.-W. Wang, T. W. Jones, M. Grigore, A. Cook, D. W. deQuilettes, R. Brenes, B. C. Duck, K. F. Anderson, N. W. Duffy, B. Wenger, V. Bulović, J. Pu, J. Li, B. Chi, H. J. Snaith and G. J. Wilson, *J. Mater. Chem. A*, 2019, **7**, 25511–25520.
27 M. Yang, T. Tian, Y. Fang, W.-G. Li, G. Liu, W. Feng, M. Xu and W.-Q. Wu, *Nat. Sustainability*, 2023, **6**, 1455–1464.
28 X. Zhu, J. Xu, H. Cen, Z. Wu, H. Dong and J. Xi, *Nanoscale*, 2023, **15**, 5167–5180.
29 J. Jin, Z. Zhu, Y. Ming, Y. Zhou, J. Shang, S. Wang, X. Cui, T. Guo, D. Zhang, G. Tang, Q. Lin, J. Li, X. Liu, S. Liu, Z. Chen, Z. Hu, H. Meng and Q. Tai, *Nat. Commun.*, 2025, **16**, DOI: 10.1038/s41467-024-55652-6.